Automated Pointing of Cardiac Imaging Catheters

Paul M. Loschak, Laura J. Brattain, and Robert D. Howe

***Abstract*— Intracardiac echocardiography (ICE) catheters enable high-quality ultrasound imaging within the heart, but their use in guiding procedures is limited due to the difficulty of manually pointing them at structures of interest. This paper presents the design and testing of a catheter steering model for robotic control of commercial ICE catheters. The four actuated degrees of freedom (4-DOF) are two catheter handle knobs to produce bi-directional bending in combination with rotation and translation of the handle. An extra degree of freedom in the system allows the imaging plane (dependent on orientation) to be directed at an object of interest. A closed form solution for forward and inverse kinematics enables control of the catheter tip position and the imaging plane orientation. The proposed algorithms were validated with a robotic test bed using electromagnetic sensor tracking of the catheter tip. The ability to automatically acquire imaging targets in the heart may improve the efficiency and effectiveness of intracardiac catheter interventions by allowing visualization of soft tissue structures that are not visible using standard fluoroscopic guidance. Although the system has been developed and tested for manipulating ICE catheters, the methods described here are applicable to any long thin tendon-driven tool (with single or bi-directional bending) requiring accurate tip position and orientation control.**

I. Introduction

Cardiologists use catheters to perform a growing range of cardiac procedures, including arrhythmia ablation, balloon angioplasty, and stent placement [1]. More complex procedures are difficult to perform with catheters due to fast heart motion and a lack of effective and easy to use imaging. Imaging is an especially vital source of feedback for cardiologists due to the limited tactile feedback in catheter procedures. At present, visualization of catheters within the heart relies largely on x-ray based fluoroscopic imaging, which exposes patients and staff to radiation and has limited ability to visualize soft tissues. In some procedures, intra-cardiac echocardiography (ICE) catheters are used to image soft tissue structures. These devices have an ultrasound array transducer in the tip of a steerable catheter, which transmits images to the clinician at real time. This approach can increase safety and effectiveness due to its ability to directly visualize the tissue structures that are the targets of many procedures. ICE also has the advantage of being minimally-invasive, portable, and more cost effective than fluoroscopy.

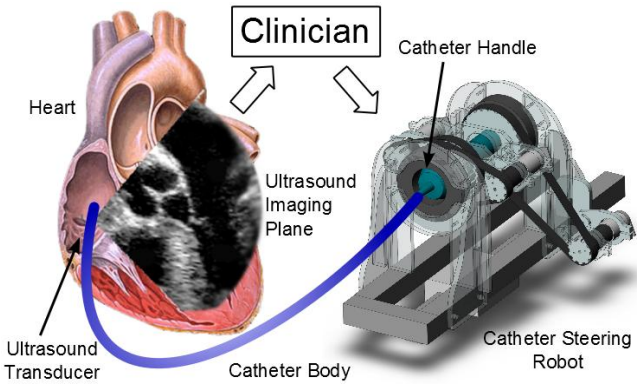

Figure 1: Imaging catheter robotic steering system

The use of ICE imaging is limited, however, because it is highly challenging to manually point the imaging plane at regions of interest within the heart. Catheter steering is accomplished using control knobs that bend the catheter tip in two directions, handle rotation, and handle translation (insertion). The relationship between these controls and the image plane location orientation is complex, particularly because the catheter shaft follows a tortuous path through the vasculature between the handle and the ultrasound transducer. This increases procedure times and largely limits ICE catheter use to critical phases of certain procedures, e.g. transseptal puncture in atrial fibrillation ablation [1].

This paper proposes the use of robotic techniques to overcome the difficulties in manually pointing ICE catheters. A kinematic model can describe the relationship between the catheter controls, tip location, and imaging plane orientation. Electromagnetic sensors on the catheter tip can determine the image location within the heart in Cartesian coordinates. Actuators can then drive the control knobs and handle position to move the catheter tip to image a region of interest or to track a working catheter.

The proposed system provides different functionality than current commercial catheter robots. These systems, such as the Amigo from Catheter Robotics, CorPath from Corindus, Artisan from Hansen Medical, and EPOCH from Stereotaxis [2-7] enable teleoperation of catheter controls to increase operator comfort and reduce exposure to radiation from fluoroscopic imaging. Some of these systems can be used with ICE catheters, but most systems are interfaced in control knob "joint space," which does not mitigate the difficulties of aiming imaging catheters using direct manual control. Existing systems controlled in Cartesian coordinates do not feature orientation control.

This paper begins with the development of a novel model that relates catheter control actions with catheter tip locations

Harvard University work is supported by the US National Institutes of Health under grant NIH R01 HL073647. MIT Lincoln Laboratory work is sponsored by the Department of the Air Force under Air Force contract #FA8721-05-C-0002. Opinions, interpretations, conclusions and recommendations are those of the authors and are not necessarily endorsed by the United States Government.

The authors are with the Harvard School of Engineering and Applied Sciences, Cambridge, MA, 02138 USA (954-644-0189; e-mail: Loschak@seas.harvard.edu). L. Brattain is also with MIT Lincoln Laboratory (e-mail: brattain@seas.harvard.edu). R.D. Howe is also with the Harvard-MIT Division of Health Sciences & Technology, Cambridge, MA 02139 USA (e-mail: howe@seas.harvard.edu).

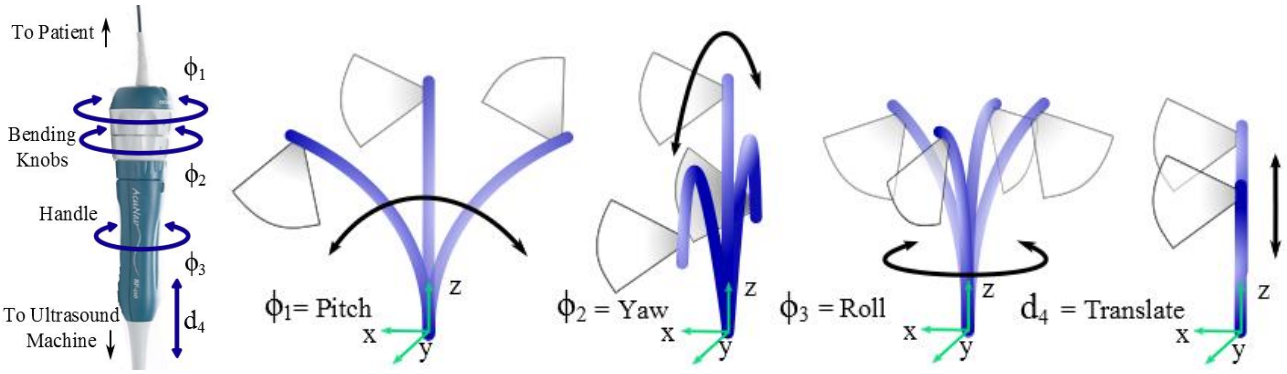

Figure 2: ICE catheter actuated degrees of freedom and corresponding tip bending directions

and ultrasound imaging plane orientations. Next, issues in catheter actuation, including joint coupling and backlash, are explored and solutions are developed. In the following section, algorithms for visualization strategies for specific tasks are created in conjunction with the bending model. Finally, we demonstrate that a 4-DOF robotic system validates the model by proving its ability to automatically point ICE catheters at the desired target. This will help clinicians to quickly achieve the needed views during procedures while reducing patient and staff exposure to radiation and reducing procedure times.

II. KINEMATICS

A. System Strategy and Design

ICE catheters are steerable catheters that acquire ultrasound images of adjacent tissues from the distal tip. They can be guided through the vasculature to the inside of the heart, where they can provide excellent views of fast moving heart structures with resolution that may not be possible with external probes. ICE can also be used for continuous monitoring of radiofrequency energy delivery during cardiac ablation [8]. The catheter consists of a plastic handle that can be rotated about or translated along its axis. Four pull wires (spaced 90 degrees apart in cross section) extend along the length of the catheter body through the bending section to their attachment points at the distal tip. On the proximal end, each pair of opposing pull wires connects to a bending knob. The bending section is designed to be less rigid than the body such that pull wire deflection causes most bending to occur in that region. The distal 2 cm tip of the catheter is rigid and contains the ultrasound transducer. A typical ICE catheter used for system validation is typical 8 Fr (2.70 mm diameter) 110 cm long catheter with a 64-element 2D ultrasound transducer at its distal tip, pictured in Figure 2 (AcuNav, Biosense Webster, Diamond Bar, CA, USA).

The system proposed here for bending model validation is designed to manipulate a commercial ICE catheter with four actuated degrees of freedom. The catheter steering robot, capable of manipulating two bending directions, handle rotation, and handle translation, enables clinicians to visualize desired objects or tissue structures in the heart using the same actuated degrees of freedom as in manual manipulation. Most commercial catheters only require one bending direction (totaling 3 DOF) to reach a desired position and complete its task without regard to orientation. The ICE catheter is unique in that it features an extra bending direction in order to achieve desired tip orientations for imaging purposes. The system's extra DOF may be utilized differently depending on the task. For instance, a user may wish to reach a desired location (with unspecified orientation) in the heart using 3 DOF and then use the extra DOF to steer the imaging plane towards a region of interest. Another task of interest is to spin the catheter tip about its own axis, thereby sweeping the imaging plane across a desired region, while keeping the catheter tip in the same location. Additionally, the user may image an object from various sides to determine an optimum viewpoint. To demonstrate this task we aim to circle an object while keeping the imaging plane pointed at the object.

Several kinematic strategies focused on catheter positioning have already been developed, and we will use these techniques as the basis of our approach to control the ICE catheter [9-11]. Additionally, researchers have also described the bending characteristics of long deformable objects, known as remotely actuated continuum robots [12, 13]. However, catheter tip orientation has not yet become a focus of investigation even though the development of robotically controlled catheter position and orientation could enable more complicated procedures to be performed in a minimally invasive fashion.

B. Forward Kinematics

This paper describes a kinematic model based on geometric principles and classic robot kinematics. Closed-form kinematic solutions have been derived for both the forward and inverse cases. This model is unique in that it is the first model known to the authors capable of calculating both the position and orientation of the catheter tip for catheters with two bending directions. With orientation information, it is then possible to determine the location and direction of the ICE imaging plane. A primary assumption of the model assumes that catheter bending occurs in the bending plane (neglecting the effects of plastic torsion). We also assume that the catheter bends with a constant radius of curvature, which has been examined previously [12], and that dynamic effects of catheter motion are negligible due to low-speed actuation.

An additional assumption for deriving the kinematic solution to the system involves positional joint coupling in bi-directional bending. Solving for the tip orientation of a traditional serial manipulator would normally require multiplying the origin orientation by transformation matrices corresponding to roll, yaw, and pitch, in the proper order (depending on the manipulator). However, the bi-directional bending catheter is a manipulator in which pitch and yaw can

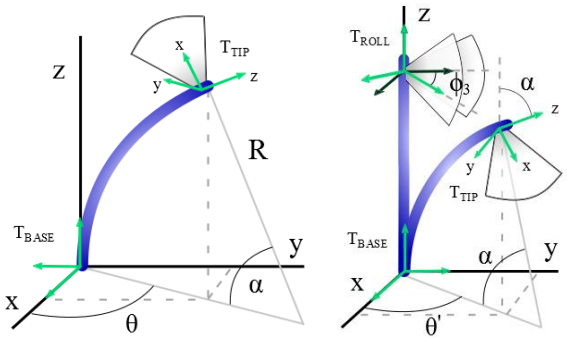

Figure 3: (a) Catheter bending geometry, (b) inverse kinematics

occur simultaneously. We begin by making the assumption that the effects of coupling between bending directions is negligible. It is assumed that applying pitch and yaw will yield the same kinematic results as applying yaw and pitch. This claim is validated in Section III.

The forward kinematics model uses the catheter handle inputs to calculate the position and orientation at the catheter tip. The catheter handle inputs correspond to the four controllable actuated degrees of freedom as in Figure 2. The first input bending knob controls pitch in the posterior-anterior plane, ϕ_1, the second input bending knob controls yaw in the right-left plane, ϕ_2, the third input is catheter handle rotation (roll), ϕ_3, and the fourth input is catheter handle translation, d_4. Knob units are radians and translation units are meters. Constants catheter radius, R_c, length of bending section, L, and effective knob diameter, D_K, must be known as well.

Intermediate variables (in Figure 3a), which describe the bending of the distal section, have been detailed by researchers in previous work [10]. The ratio of yaw to pitch, θ, is the angle between the bending plane and the X-Z plane.

$$\theta = \tan^{-1}(\phi_2/\phi_1) \tag{1}$$

The amount of pitch and yaw pull wire deflections due to the bending knobs are ΔL_1 and ΔL_2.

$$\Delta L_1 = \phi_1 D_K/2, \quad \Delta L_2 = \phi_2 D_K/2 \tag{2}$$

Curvature is described by calculating

$$\alpha = \sqrt{(\Delta L_1/R_c)^2 + (\Delta L_2/R_c)^2}. \tag{3}$$

The radius of curvature is

$$R = L/\alpha. \tag{4}$$

The catheter tip position from bending can be calculated using R, α, and θ. It should be noted here that θ and Z are calculated due to only adjustments in the bending knobs (and not handle rotation or translation). Handle rotation and translation will be applied in a later step.

$$X = R(1-\cos\alpha)\cos\theta \tag{5}$$

$$Y = R(1-\cos\alpha)\sin\theta \tag{6}$$

$$Z = R\sin\alpha \tag{7}$$

The tip orientation due to bending can be calculated by the equivalent axis theorem (8), which rotates orientation by angle α about a new axis $\mathbf{u}$ that is orthogonal to the bending plane, where $C_\alpha = \cos\alpha$, $S_\alpha = \sin\alpha$, and $V = (1 - \cos\alpha)$ [14].

The unit vector $\mathbf{u}$ is calculated by cross products of vectors relating the catheter tip to the base of the bending section and the center of the bending arc.

$$R_{TILT}(\alpha, \mathbf{u}) = \begin{bmatrix} u_1^2V\alpha + C_\alpha & u_1u_2V\alpha - u_3S_\alpha & u_1u_3V\alpha + u_2S_\alpha \\ u_1u_2V\alpha + u_3S_\alpha & u_2^2V\alpha + C_\alpha & u_2u_3V\alpha - u_1S_\alpha \\ u_1u_3V\alpha - u_2S_\alpha & u_2u_3V\alpha + u_1S_\alpha & u_3^2V\alpha + C_\alpha \end{bmatrix} \tag{8}$$

A 4x4 transformation matrix, $T_{TILT}(\phi_1, \phi_2, \mathbf{u})$, is then assembled to tilt the bending tip with respect to the bending base. This contains (8) as the rotation and values from (5)-(7) as tip position. Next, the handle rotation and translation matrices, $T_{ROLL}(\phi_3)$ and $T_{TRANS}(d_4)$, are pre-multiplied to find the final position and orientation, T_{TIP}.

$$T_{TIP} = T_{TRANS}(d_4)T_{ROLL}(\phi_3)T_{TILT}(\phi_1, \phi_2, \mathbf{u}) \tag{9}$$

C. Inverse Kinematics

The inverse kinematic model takes the catheter tip position and orientation matrix, T_{TIP}, as input and solves the single possible catheter configuration. While there are several strategies to calculate the inverse kinematics, this strategy was chosen such that the imaging plane could be specified to point in the proper plane. The model outputs the required joint angles (bending knobs, handle roll, and translation) required to achieve the desired configuration.

The z-axis of the orientation at the catheter tip is assumed to be tangent to the catheter arc. Therefore, it is possible to solve for intermediate variables α and R which describe the amount of bending in Figure 3b. Calculating the dot product of the world z-axis and the catheter tip z-axis defines the tilt.

$$\alpha = \cos^{-1}(\mathbf{z}^{WORLD} \bullet \mathbf{z}^{TIP}) \tag{10}$$

Now we must analyze rotation, but it is currently not possible to identify whether the bending plane's rotation occurred due to bending, θ, handle roll, ϕ_3, or a combination of both. Therefore in the meantime we can use the x and y values of the catheter tip to solve for θ', which will soon be used to calculate the true θ.

$$R = L/\alpha \tag{11}$$

$$\theta' = \tan^{-1}(y/x) \tag{12}$$

The equivalent axis theorem may be applied once again to rotate the tip orientation by α about an axis orthogonal to the bending plane. The orthogonal axis $\mathbf{u}'$ is used to find the true value. Applying (8) results in transforming the tip orientation to an intermediate orientation in which the new z-axis is collinear with the world frame z-axis. The resulting angle between the temporary x-axis and the world frame x-axis is the handle rotation angle, ϕ_3. In this way, we have systematically "undone" the bending to reveal the true inputs that will allow our catheter to achieve the desired configuration. With ϕ_3 we may calculate the true θ and the pull wire displacements.

$$\Delta L_1 = R_c\,\alpha/\sqrt{1+\tan^2\theta} \tag{13}$$

$$\Delta L_2 = -\tan\theta\, R_c\,\alpha/\sqrt{1+\tan^2\theta} \tag{14}$$

$$d_4 = Z_{TIP} - R\sin\alpha \tag{15}$$

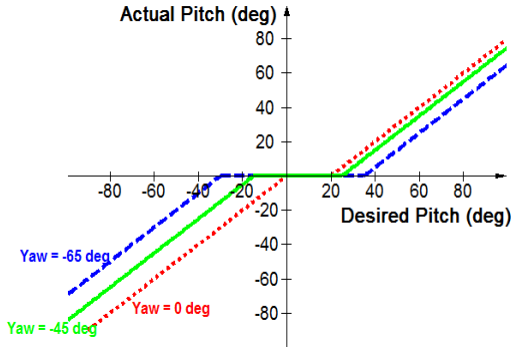

Figure 4: Dead zone mapping data

With all four catheter inputs known, converting the values to actuator space becomes trivial. The inverse kinematic function allows the system to easily input the catheter's current and desired positions and then output the required motor commands.

III. Catheter Behavior

A. Joint Coupling

Actuating two directional bending knobs raises the issue of positional joint coupling. Initial tests were done to examine these effects by evaluating whether the chronological order of joint actuation affects the final catheter tip destination. The bending space was discretized into 5° increments and actuated robotically while recording the catheter tip positions with EM trackers. First one knob remained constant while the second knob was incremented, and then the first knob was incremented while the second knob remained constant throughout the entire workspace (±90° for both knobs). Each set of points was compared and it was determined that the maximum distance between two corresponding points was within 1 mm. This closeness between points shows that positional pull wire coupling has a minimal effect on the system through most of the bending range, thus validating use of the equivalent axis theorem in kinematics modeling. Coupling effects, likely due to friction in the pull wires, were slightly more significant at high bending angles. Although we do not focus on force application in this paper, it is important to note that this system would likely experience significant joint coupling in force control.

B. Dead Zone Compensation

Most commercial catheters have an inherent dead zone when bending knobs cross the zero point due to slack in the pull wire strings and a lack of a tensioner. The slack results in a dead zone ranging roughly ±20° in which twisting the bending knobs yields zero output. In manual manipulation, humans compensate for this by feeling the tension in the knobs and use a combination of the ultrasound image and fluoroscopy to determine when motion has occurred. For the robotic case we have chosen to manage the zero-crossing point by creating a numerical map of the bending workspace. This map specifies the range in which bending knob input yields no output motion. The map can be applied for accurate knob adjustments. Figure 4 plots the dead zones in the pitch bending knob for several values of yaw. Dead zone compensation must be applied towards both increasing and decreasing knob angles in the same manner. It is important to note that the dead zone in each knob becomes wider as the other knob is further actuated. The desired knob angle, ϕ_i, is summed with the compensation angle, δ, which is dependent on the existing angle of the other knob, ϕ_j, to yield the total angular output, ϕ_i'. This relationship is given by

$$\phi_i' = \phi_i + \delta \tag{16}$$

Where $\delta = f(\phi_j)$. This occurs because actuating any subset of the bending knobs creates tension in the actuated pull wires, compression in the catheter body, and thus lengthens pull wire slack in non-actuated pull wires. Catheter body compression is an important consideration that will be examined closely in future work as the system advances towards use in the vasculature. It should also be noted that the system experiences traditional backlash when changing knob directions, but these effects are significantly smaller than the resolution of the map used for dead zone compensation and therefore may be neglected.

C. Controller

A kinematics-based closed-loop controller in Figure 5 was used for maximizing system performance. The commanded catheter tip position and orientation, X_{COM}, are input to the inverse kinematics model to calculate the four control variables in joint space, q^*. The bending knob inputs are adjusted by compensating for the dead zone at the zero-crossings of the bending knobs and then all joint space variables are converted to motor commands. A fast motor controller feedback loop confirms that the correct actuator motion has been achieved. EM tracker measurements of catheter tip position and orientation are compared with the desired inputs and multiplied by gains to input a new commanded value. This feedback loop updates the commanded motion based on the catheter tip's current and desired locations until the desired configuration is reached. The gains were determined experimentally.

IV. Experiments

A. Robot Design

The robot pictured in Figure 6 was constructed to actuate the catheter handle knobs and provide the four DOF used in

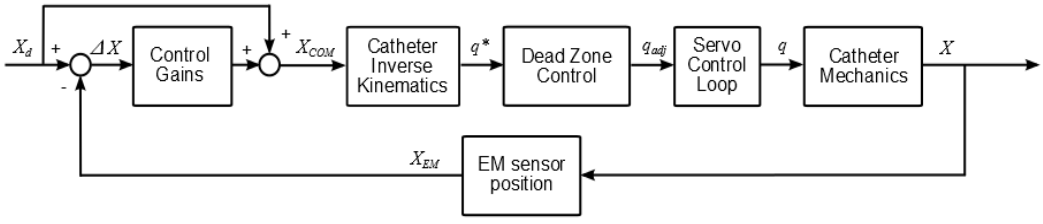

Figure 5: Kinematics-based closed-loop task space control diagram

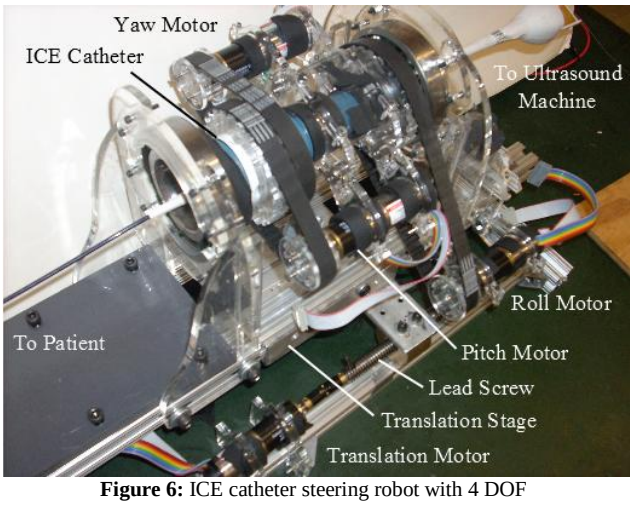

Figure 6: ICE catheter steering robot with 4 DOF

the model. Each DOF was actuated by 6.5 W brushed motors driven by digital positioning controllers (Maxon Motor, Sachseln, Switzerland). Two actuators were mounted to the catheter handle and connected to the knobs by timing belts. Gears for the timing belts were designed to manipulate the handle's 3D geometry. The catheter handle (with actuators) was suspended by two ball bearings, allowing rotation about the handle center axis. A third actuator was connected to the catheter handle by a timing belt to provide handle rotation. The entire system was mounted to a lead screw driven translation stage. For initial testing, a plastic holder was designed to support the distal 7 cm of catheter length roughly 1 m away from the handle while still allowing free rotation about the handle axis.

B. Spinning the catheter about its axis

The first experimental task was to use the system's extra DOF to spin the imaging plane of the catheter about the axis of the catheter while in bending. During manual manipulation, a clinician may wish to steer the ICE catheter tip into a desired region of the heart and sweep the imaging plane to get a comprehensive view of the region. While in bending, it is extremely difficult to intuitively and manually spin the catheter about its own axis while keeping the tip in place. Here the catheter robot has the opportunity to use its redundant DOF to accomplish this task. The user may automatically or manually navigate the catheter to the desired region of the heart and then input the desired range of angles to sweep with a specified angular resolution. Rotations about the z-axis by angle ψ are applied to the tip's mobile coordinate frame as in (18) by post-multiplication and the resulting configurations are input to the inverse kinematics to solve for the corresponding joint variables.

$$T_{SPIN} = \begin{bmatrix} \cos\psi & -\sin\psi & 0 \\ -\sin\psi & \cos\psi & 0 \\ 0 & 0 & 1 \end{bmatrix} \quad (17)$$

$$T_{SPIN_i} = T_{TIP} T_{SPIN} \quad (18)$$

The ICE catheter was commanded to spin about its own axis and sweep the imaging plane through a range of -45° to 45° in 12 steps while keeping the tip position in the same physical location. A schematic of the imaging plane motion is in Figure 7a. The joint variables calculated by inverse kinematics to achieve the desired sweeping are plotted in Figure 7b. The measured orientations of the catheter tip at each step are plotted in Figure 7c. The first imaging plane angle and the last imaging plane angle (denoted by the change in line brightness) show that the imaging plane swept through the desired range. Accuracy of this task is measured by the catheter's ability to sweep through the desired range of imaging plane orientations while maintaining a fixed *x-y-z* position at the tip. The catheter tip position experienced small fluctuations that were limited to within 6 mm in all directions.

C. Visualizing an object from all sides

The second experimental task was to use the redundant DOF to rotate the catheter tip around an object while keeping the image plane pointed at the object, as in Figure 8a. To demonstrate this technique, the ICE catheter was made to circle around an object with an EM tracker at a focal distance, F_D, and accurately aim the imaging plane at the target. The catheter trajectory was determined by calculating the appropriate bending angle given the focal distance constraint as in Figure 8b. Equations (4), (5), and the cosine of the bending angle were combined to yield (19).

$$F_D \cos\alpha = \frac{L}{\alpha}(1 - \cos\alpha) = R_{TRAJ} \quad (19)$$

This can be solved numerically to find the value for α which satisfies the equation. Then we can calculate the radius of the circular trajectory, R_{TRAJ}, at which the catheter may rotate about the object while visualizing it in the imaging plane and maintaining a fixed distance. Once the trajectory is defined, each position and orientation may be passed through the inverse kinematics function to determine the proper joint

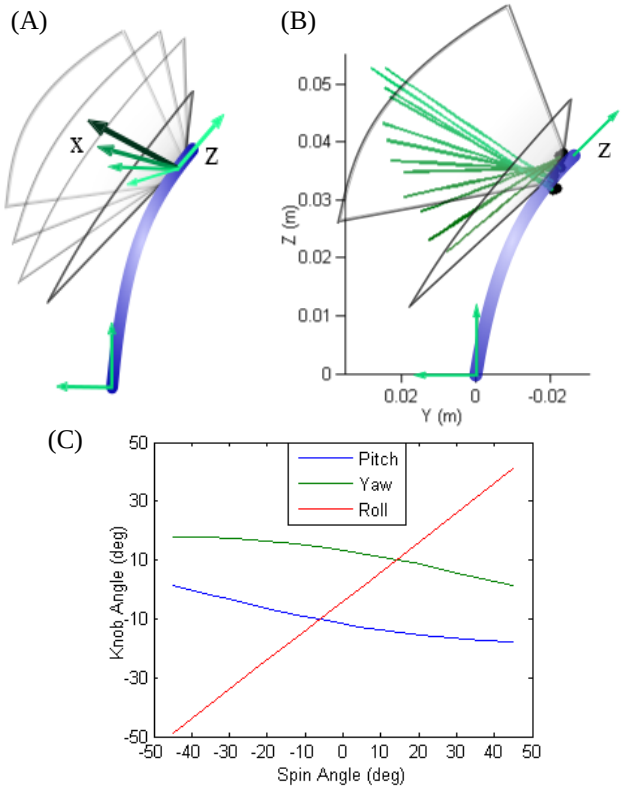

Figure 7: (a) Simulation showing the catheter spinning about its own axis, (b) spinning test results with blue lines to represent the imaging plane axis rotation, (c) joint angles required to actuate motion

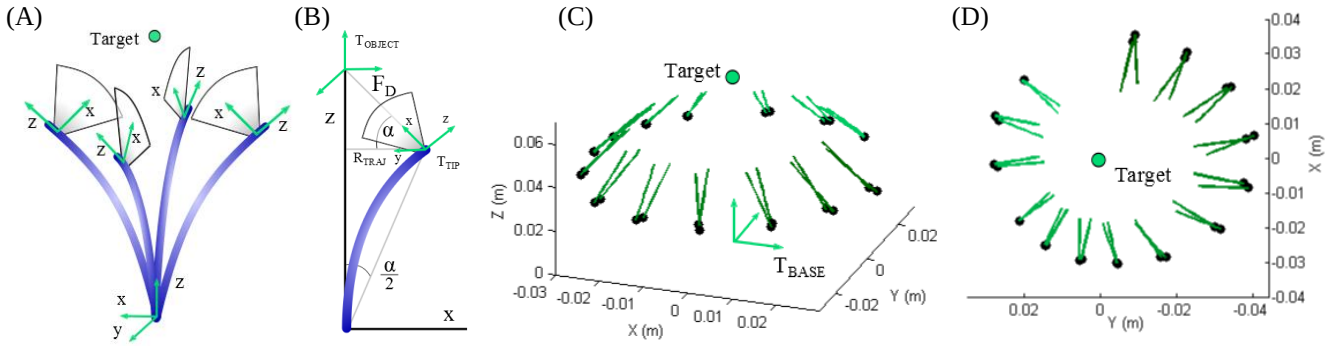

Figure 8: (a) Simulation showing the catheter circling an object while keeping its imaging plane pointed towards the target, (b) calculations for circling an object, (c) imaging plane results before and after angular adjustment, (d) imaging planes facing towards object (top view)

variables. The catheter was made to reach 14 locations around the object while pointing at the object. The feedback loop made small adjustments at each location to spin the orientation until the imaging plane pointed directly at the object. Mechanical restraints limited the robot's handle rotation joint to roughly ±175°, preventing the catheter from making a full 360° circle around the object. Figures 8c and 8d show catheter tip measurements including each point around the circle before and after adjusting the imaging plane. Figure 8d shows the circular trajectory from the top, highlighting the accuracy with which the catheter aligns its imaging plane to point at the target. The average imaging plane alignment error was 0.031 radians (1.7°).

These experiments demonstrate the fine positioning and rotational accuracy of the system in conjunction with using a redundant DOF to obtain useful imaging techniques. Since heart anatomy poses many constraints on catheter motion, these techniques are useful for controlling the position and orientation of the imaging plane to visualize interactions with tissue. For example, a clinician could monitor a working catheter's interactions with tissue by rotating around the working catheter to achieve the desired view. Or, by simply having the clinician indicate the desired view, the ICE catheter would then be robotically driven to image the desired plane.

V. Conclusions

Clinicians using ICE catheters currently express frustration at the need to frequently adjust their ICE catheters to track the non-imaging catheters and their interactions with surrounding tissue. Therefore, controlling the position and orientation of the catheter tip and the imaging plane is essential for improving current catheter-based procedures and enabling more procedures to be done in a minimally invasive way. In this paper we presented a system that automatically steers a 4-DOF imaging catheter to align its imaging plane to a desired orientation. The kinematic model used by the system may also be useful for the development of catheter tools and procedures that rely on achieving a designated orientation with respect to the tissue. Future work on this preliminary system will incorporate optimization techniques for safety and trajectory planning, examine the effects of pull wire friction, and determine strict boundary limits for catheter movement due to heart anatomy. With the incorporation of real time ultrasound visualization and image processing, the robot will be able to process images of heart structures and use inverse kinematics to navigate the catheter tip and imaging plane while maintaining specific relationships with other objects in the heart. Robotic control of ICE could greatly shorten procedure times, improve patient outcomes, and reduce the training time required to master ICE.

Acknowledgment

The authors would like to acknowledge Samuel B. Kesner, PhD, Yaroslav Tenzer, PhD, and Frank Hammond III PhD, for helpful discussions on system design and Elad Anter, MD, for helpful discussions about ICE.

References

[1] D. S. Baim, *Grossman's Cardiac Catheterization, Angiography, and Intervention*, Lippincott Williams & Wilkins, 2005, pp.992.
[2] Catheter Robotics, Inc. *Amigo Remote Catheter System* [PDF]. Available: http://www.catheterrobotics.com
[3] Corindus, Inc. *Robotic-Assisted PCI CorPath 200 System* [PDF]. Available: http://www.corindus.com
[4] Hansen Medical, Inc. *Sensei X Robotic Catheter System* [PDF]. Available: http://www.hansenmedical.com
[5] A. B. Koolwal, F. Barbagli, C. R. Carlson, and D. H. Liang, "A fast SLAM approach to freehand 3-D ultrasound reconstruction for catheter ablation guidance in the left atrium," *Ultrasound in Medicine and Biology*, vol. 37, no. 12, pp. 2037-2054, 2011.
[6] Stereotaxis. *Niobe ES* [Online]. Available: http://www.stereotaxis.com
[7] F. M. Creighton, IV, R. C. Ritter, R. R. Viswanathan, N. Kastelein, J. M. Garibaldi, W. Flickinger, "Operation of a remote medical navigation system using ultrasound image," U.S. Patent Application US2009/0062646 A1, filed Sept. 5, 2008.
[8] Intracardiac Echocardiography [Online] Available: http://www.eplabdigest.com/article/4148
[9] D. B. Camarillo, C. F. Milne, C. R. Carlson, Michael R. Zinn, and J. K. Salisbury, "Mechanics modeling of tendon-driven continuum manipulators," *IEEE Trans. on Robotics*, vol. 24, no. 6, pp. 1262-1273, 2008.
[10] R. S. Penning, J. Jung, J. A. Borgstadt, N. J. Ferrier, M. R. Zinn, "Towards closed loop control of a continuum robotic manipulator for medical applications," in Proc. IEEE Int. Conf. Robotics and Automation, pp. 4822-4827, 2011.
[11] Y. Ganji, F. Janabi-Sharifi, A. N. Cheema, "Robot-assisted catheter manipulation for intracardiac navigation," Int. J. Computer Assisted Radiology and Surgery, vol. 4, pp. 307-315, 2009.
[12] I. A. Gravagne, C. D. Rahn, I. D. Walker, "Large deflection dynamics and control for planar continuum robots," *IEEE/ASME Trans. on Mechatronics*, vol. 8, no. 2, pp. 299-307, 2003.
[13] D. C. Rucker, R. J. Webster, III, "Statics and dynamics of continuum robots with general tendon routing and external loading," IEEE Trans. on Robotics, vol. 27, no. 6, pp. 1033-1044, 2011.
[14] R. J. Schilling, "Direct Kinematics: The Arm Equation," *Fundamentals of Robotics Analysis and Control*, Englewood Cliffs, New Jersey: Prentice-Hall, 1990, ch. 2, sec. 2-3, pp. 38-40.